Kohn Anomalies and Electron-Phonon Interactions in Graphite

S. Piscanec,[1] M. Lazzeri,[2] Francesco Mauri,[2] A. C. Ferrari,[1] and J. Robertson[1]

[1]*Cambridge University, Engineering Department, Trumpington Street, Cambridge CB2 1PZ, United Kingdom*
[2]*Laboratoire de Minéralogie-Cristallographie de Paris, 4 Place Jussieu, 75252, Paris cedex 05, France*

(Received 23 April 2004; published 28 October 2004)

We demonstrate that graphite phonon dispersions have two Kohn anomalies at the Γ-E_{2g} and $\mathbf{K}$-A_1' modes. The anomalies are revealed by two sharp kinks. By an exact analytic derivation, we show that the slope of these kinks is proportional to the square of the electron-phonon coupling (EPC). Thus, we can directly measure the EPC from the experimental dispersions. The Γ-E_{2g} and $\mathbf{K}$-A_1' EPCs are particularly large, while they are negligible for all the other modes at Γ and $\mathbf{K}$.

DOI: 10.1103/PhysRevLett.93.185503 PACS numbers: 63.20.Dj, 63.20.Kr, 71.15.Mb, 78.30.–j

Carbon nanotubes (CNTs) are at the core of nanotechnology research. They are prototype one-dimensional conductors. Metallic nanotubes are predicted to be one-dimensional quantum wires with ballistic electron transport [1]. However, high field transport measurements show that the electron-phonon scattering by optical phonons at $\mathbf{K}$ and Γ breaks down the ballistic behavior [2]. Electron-phonon coupling (EPC) is thus the fundamental bottleneck for ballistic transport. Raman spectroscopy is a prime characterization technique to identify CNTs in terms of their size and electronic properties [3]. The optical phonons at $\mathbf{K}$ and Γ are the phonons responsible for the Raman D and G peaks in carbons [4]. The frequency and the intensity of the Raman modes are determined by the EPC matrix elements [5]. The determination of the EPCs is necessary to settle the 35-year debate on the nature of the Raman D peak in carbons [4–12]. Finally, although graphite phonon dispersions have been widely studied, several contrasting theoretical dispersions were proposed [6–10,13,14]. In particular, the origin of the large overbending of the $\mathbf{K}$-A_1' branch is not yet understood and is associated with an intense EPC [4,9,10]. In principle, the electronic and vibrational properties of CNTs can be described by folding the electronic and phonon dispersions of graphite. The determination of the graphite EPCs is thus the crucial step in understanding the properties of any carbon based material and CNTs, in particular. It is then surprising that, despite the vast literature on carbon materials, no experimental determination or first principle calculations of the graphite EPCs has been done so far, to the best of our knowledge.

Here we show that in graphite the EPC matrix elements at Γ and $\mathbf{K}$ can be directly extracted from the phonon dispersions. We demonstrate two remarkable Kohn anomalies in the phonon dispersions at Γ and $\mathbf{K}$, by an exact analytic derivation and accurate density functional theory (DFT) calculations. We prove that the slope of the anomalies is proportional to the EPC square.

A key feature of graphite is the semimetallic character of the electronic structure. In general, the atomic vibrations are partially screened by electrons. In a metal this screening can change rapidly for vibrations associated with certain $\mathbf{q}$ points of the Brillouin zone (BZ), determined by the shape of the Fermi surface. The consequent anomalous behavior of the phonon dispersion is called Kohn anomaly [15]. Kohn anomalies may occur only for $\mathbf{q}$ such that there are two electronic states $\mathbf{k}_1$ and $\mathbf{k}_2 = \mathbf{k}_1 + \mathbf{q}$ both on the Fermi surface [15]. The electronic bands dispersions of graphite are, essentially, described by those of an isolated graphene sheet. In graphene, the electronic gap is zero only at the two equivalent BZ points $\mathbf{K}$ and $\mathbf{K}'$. Since $\mathbf{K}' = 2\mathbf{K}$, the two equivalent $\mathbf{K}$ points are connected by the vector $\mathbf{K}$. Thus, Kohn anomalies can occur for $\mathbf{q} = \Gamma$ or $\mathbf{q} = \mathbf{K}$.

We perform calculations within the generalized gradient approximation (GGA) [16], using the density functional perturbation theory (DFPT) scheme [17], which allows the exact (within DFT) computation of phonon frequencies at any BZ point. We use the plane waves (90 Ry cutoff) and the pseudopotential [18] approach. The electronic levels are occupied with a finite *fictitious* electronic temperature σ [19]. This smears out the discontinuities present in the Fermi distribution for $\sigma = 0$, and the exact result is recovered for $\sigma \to 0$. The experimental lattice ($a_{\mathrm{exp}} = 2.46$ Å, $c = 6.708$ Å) is used for graphite, while for graphene we consider both the graphite a_{exp} and the theoretical values ($a_{\mathrm{th}} = 2.479$ Å). Graphene layers are separated by 7.4 Å of vacuum.

Figure 1 compares the measured optical branches [9] with our calculations at $\sigma = 0.02$ Ry. Phonon frequencies are computed exactly for a series of points along the high symmetry lines Γ-$\mathbf{K}$ and Γ-$\mathbf{M}$ and then are interpolated with a spline. The agreement with experiments is $\sim$2%, which is the expected accuracy of DFT-GGA. At Γ the experimental dispersion is very well reproduced by the calculations with a_{exp}. At $\mathbf{K}$ the upper branch is better described by the calculations with a_{th}.

The most striking feature of these dispersions is the discontinuity in the frequency derivative of the highest optical branches (HOBs) at Γ and at $\mathbf{K}$ (E_{2g} and A_1' modes). Indeed, near Γ, $\hbar\omega_{\mathbf{q}} = \alpha_\Gamma q + \hbar\omega_\Gamma + \mathcal{O}(q^2)$,

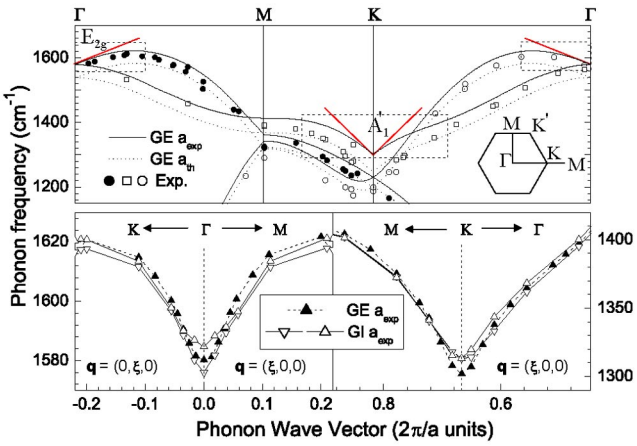

FIG. 1 (color online). Upper panel: lines: phonon dispersion of graphene (GE), calculated at the experimental and equilibrium lattice spacings (a_{exp} and a_{th}). Points: experimental data from Ref. [9]. The red straight lines at Γ and **K** are obtained from Eqs. (8) and (10). The two lower panels correspond to the dotted windows in the upper panel. The points are theoretical frequencies obtained by direct calculation. A single graphene band corresponds to two almost degenerate graphite (GI) bands.

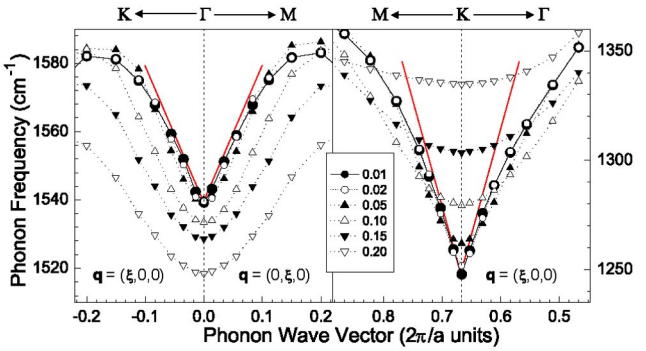

FIG. 2 (color online). Graphene HOB around Γ and **K** as a function of smearing. Points are calculated frequencies for a_{th}. Lines are guides to the eye. The red straight lines plot Eqs. (8) and (10).

with $\omega_{\mathbf{q}}$ being the phonon frequency of the HOB at the **q** wave vector. Similarly, near **K**, $\hbar\omega_{\mathbf{K}+\mathbf{q}'} = \alpha_{\mathbf{K}} q' + \hbar\omega_{\mathbf{K}} + \mathcal{O}(q'^2)$. Such dependencies cannot be described by a finite set of interatomic force constants, or by a set decaying exponentially with the real-space distance. In these cases the dynamical matrix dependence on **q** would be analytic, and, because of symmetry, *the highest optical branch near* Γ *and* **K** *would have a flat slope* ($\alpha_\Gamma = \alpha_{\mathbf{K}} = 0$). Thus, a non zero α_Γ or $\alpha_{\mathbf{K}}$ indicates a nonanalytic behavior of the phonon dispersion, due to a polynomial decay of the force constants in real space. This explains why it is impossible for any of the often used few-nearest-neighbor force constants approaches to properly describe the HOB phonons near **K** and Γ [6–8,10,13,14]. The graphite HOBs are almost indistinguishable from those of graphene, Fig. 1. In particular, the nonanalytic behavior at Γ and **K** is also present in graphite. At Γ the HOB is doubly degenerate, consisting of in-plane antiphase E_{2g} movements. Near Γ the two modes split in a upper longitudinal optical (LO) branch and a lower transverse optical (TO) branch. $\alpha_\Gamma \neq 0$ only for the LO.

Figure 2 plots the HOBs as a function of σ, to clarify the nature of the discontinuities. The results for $\sigma = 0.01$ Ry and $\sigma = 0.02$ Ry are similar, indicating that, on the scale of the figure, the $\sigma \to 0$ limit is reached. Increasing σ, the nonanalytic behavior is smoothed out. Particularly striking is the behavior around **K**, where for $\sigma > 0.20$ Ry the dispersion is almost flat. Within DFPT, the smearing σ affects virtual transitions between occupied and empty states, differing in energy $\lesssim \sigma$. Thus, the smoothing of Fig. 2 indicates that the HOB discontinuities are Kohn anomalies [15], since they are due to an anomalous screening of the electrons around the Fermi energy.

We compute the EPC matrix elements to understand why the Kohn anomalies affect only the HOBs and not the others. For a given phonon mode at the reciprocal-space point **q**, we call $\Delta V_{\mathbf{q}}$ and $\Delta n_{\mathbf{q}}$ the derivative of the Kohn-Sham potential and of the charge density, with respect to a displacement along the normal coordinate of the phonon. We define

$$g_{(\mathbf{k}+\mathbf{q})i,\mathbf{k}j} = \langle \mathbf{k}+\mathbf{q}, i|\Delta V_{\mathbf{q}}[\Delta n_{\mathbf{q}}]|\mathbf{k}, j\rangle\sqrt{\hbar/(2M\omega_{\mathbf{q}})}, \quad (1)$$

where we consider explicitly the dependence of $\Delta V_{\mathbf{q}}$ on $\Delta n_{\mathbf{q}}$, as indicated by $\Delta V_{\mathbf{q}}[\Delta n_{\mathbf{q}}]$. $|\mathbf{k}, i\rangle$ is the electronic Bloch eigenstate with wave vector **k**, band index i, and eigenenergy $\epsilon_{\mathbf{k},i}$. M is the atomic mass and g is an energy. The dimensionless EPC is $\lambda_{\mathbf{q}} = 2\sum_{\mathbf{k},i,j} \times |g_{(\mathbf{k}+\mathbf{q})i,\mathbf{k}j}|^2 \delta(\epsilon_{\mathbf{k}+\mathbf{q},i} - \epsilon_{\mathrm{F}})\delta(\epsilon_{\mathbf{k},j} - \epsilon_{\mathrm{F}})/(\hbar\omega_{\mathbf{q}} N_{\mathrm{F}} N_{\mathrm{k}})$, where $\sum_{\mathbf{k}}$ is a sum on N_{k} BZ vectors, N_{F} is the density of states per spin at the Fermi energy ϵ_{F}. In graphene the Fermi surface is a point, N_{F} is zero, and $\lambda_{\mathbf{q}}$ is not well defined. Thus, we evaluate $2\langle g^2_{\mathbf{q}}\rangle_{\mathrm{F}}/(\hbar\omega_{\mathbf{q}}) = \lambda_{\mathbf{q}} N_{\mathrm{F}}/J_{\mathbf{q}}$, where $\langle \ldots \rangle_{\mathrm{F}}$ indicates the average on the Fermi surface of $|g_{(\mathbf{k}+\mathbf{q})i,\mathbf{k}j}|^2$, and $J_{\mathbf{q}} = 1/N_k \sum_{i,j,\mathbf{k}} \delta(\epsilon_{\mathbf{k}+\mathbf{q},i} - \epsilon_{\mathrm{F}})\delta(\epsilon_{\mathbf{k},j} - \epsilon_{\mathrm{F}})$. In graphene, $\langle g^2_{\mathbf{K}}\rangle_{\mathrm{F}} = \sum^{\pi}_{i,j} |g_{(2\mathbf{K})i,\mathbf{K}j}|^2/4$, and $\langle g^2_{\Gamma}\rangle_{\mathrm{F}} = \sum^{\pi}_{i,j} |g_{\mathbf{K}i,\mathbf{K}j}|^2/4$, where the sums are performed on the two degenerate π bands at ϵ_{F}. For the HOBs, we obtain $\langle g^2_{\Gamma}\rangle_{\mathrm{F}} = 0.0405$ eV^2, and $\langle g^2_{\mathbf{K}}\rangle_{\mathrm{F}} = 0.0994$ eV^2, corresponding to $2\langle g^2_{\mathbf{q}}\rangle_{\mathrm{F}}/(\hbar\omega_{\mathbf{q}})$ of 0.41 and 1.23 eV at Γ and **K**, respectively. $2\langle g^2_{\mathbf{K}}\rangle_{\mathrm{F}}/(\hbar\omega_{\mathbf{K}})$ is much smaller (0.02 eV) for the doubly degenerate 1200 cm^{-1} phonon at **K** and zero for all the other phonons at **K** and at Γ, consistent with the absence of Kohn anomalies for all these branches. The EPC values for the graphene HOBs are very large. They are comparable to the 39 K superconductor MgB_2, for which $\lambda_{\mathbf{q}} N_{\mathrm{F}}/J_{\mathbf{q}} = 1.6$ eV [20] for each of the two strongly-coupled E_{2g} branches at A.

We consider the expression of $\omega_{\mathbf{q}}$ according to perturbation theory [17] (within DFT), to understand the absence of a Kohn anomaly for the TO E_{2g} phonon at Γ and to correlate the constants α_Γ and $\alpha_{\mathbf{K}}$ with the magnitude of the EPC. $\omega_{\mathbf{q}} = \sqrt{D_{\mathbf{q}}/M}$, where $D_{\mathbf{q}}$ is the dynamical matrix projected on the phonon normal coordinate

$$D_{\mathbf{q}} = \frac{4}{N_{\mathrm{k}}} \sum_{\mathbf{k},o,e} \frac{|\langle \mathbf{k}+\mathbf{q}, e|\Delta V_{\mathbf{q}}[\Delta n_{\mathbf{q}}]|\mathbf{k}, o\rangle|^2}{\epsilon_{\mathbf{k},o} - \epsilon_{\mathbf{k}+\mathbf{q},e}} - \int \Delta n^*_{\mathbf{q}}(\mathbf{r}) K(\mathbf{r},\mathbf{r}') \Delta n_{\mathbf{q}}(\mathbf{r}') d^3r d^3r' + \int n(\mathbf{r}) \Delta^2 V^b(\mathbf{r}) d^3r. \quad (2)$$

Here a factor of 2 accounts for spin degeneracy, $\sum_{o,e}$ is a sum on occupied and empty states, $n(\mathbf{r})$ is the charge density, $K(\mathbf{r},\mathbf{r}') = \delta^2 E_{\mathrm{Hxc}}[n]/(\delta n(\mathbf{r})\delta n(\mathbf{r}'))$, $E_{\mathrm{Hxc}}[n]$ is the Hartree and exchange-correlation functional, and $\Delta^2 V^b$ is the second derivative of the bare (purely ionic) potential. From previous considerations,

$$\alpha_\Gamma = \hbar \lim_{\mathbf{q}\to 0} \frac{\omega_{\mathbf{q}} - \omega_\Gamma}{q} = \hbar \lim_{\mathbf{q}\to 0} \frac{D_{\mathbf{q}} - D_\Gamma}{2M\omega_\Gamma q}, \quad (3)$$

$$\alpha_{\mathbf{K}} = \hbar \lim_{\mathbf{q}'\to 0} \frac{\omega_{\mathbf{K}+\mathbf{q}'} - \omega_{\mathbf{K}}}{q'} = \hbar \lim_{\mathbf{q}'\to 0} \frac{D_{\mathbf{K}+\mathbf{q}'} - D_{\mathbf{K}}}{2M\omega_{\mathbf{K}} q'}. \quad (4)$$

If the dependence of $D_{\mathbf{q}}$ on $\mathbf{q}$ were analytic over all the BZ, $\alpha_\Gamma = \alpha_{\mathbf{K}} = 0$ [e.g,. $D_{\mathbf{q}} - D_\Gamma = \mathcal{O}(q^2)$]. For $\mathbf{q} \neq \Gamma$ and $\mathbf{K}$, the denominators in the sum of Eq. (2) are finite and $D_{\mathbf{q}}$ is analytic. The denominators go to zero for $\mathbf{q} = \Gamma$ (when $\mathbf{k} = \mathbf{K}$ or $\mathbf{k} = 2\mathbf{K}$) and for $\mathbf{q} = \mathbf{K}$ (when $\mathbf{k} = \mathbf{K}$), when o and e correspond to the π and π^* bands near the Fermi energy. Because of these singularities, the dynamical matrix is nonanalytic for $\mathbf{q} = \mathbf{K}, \Gamma$, thus α_Γ and $\alpha_{\mathbf{K}}$ can be different from zero. To compute $\alpha_{\mathbf{q}}$, we can replace in Eqs. (3) and (4) the full dynamical matrix $D_{\mathbf{q}}$ with its nonanalytic component $\tilde{D}_{\mathbf{q}}$, which includes only the sum of Eq. (2) restricted to the π electronic bands in an arbitrarily small but finite circle of radius k_{m} around the Fermi surface at the $\mathbf{K}$ and/or $2\mathbf{K}$ points [21].

For $\mathbf{q}$ near Γ, using the definition of Eq. (1),

$$\tilde{D}_{\mathbf{q}} = \frac{8\sqrt{3}M\omega_\Gamma}{\hbar} \int_{k'<k_{\mathrm{m}}} d^2k' \frac{|g_{(\mathbf{K}+\mathbf{k}'+\mathbf{q})\pi^*,(\mathbf{K}+\mathbf{k}')\pi}|^2}{\epsilon_{\mathbf{K}+\mathbf{k}',\pi} - \epsilon_{\mathbf{K}+\mathbf{k}'+\mathbf{q},\pi^*}}. \quad (5)$$

Here we have used the substitution $1/N_{\mathrm{k}}\sum_{\mathbf{k}} = \sqrt{3}/2 \int d^2k'$ (the graphene BZ area is $2/\sqrt{3}$); $\mathbf{q}$ and $\mathbf{k}$ points are in units of $2\pi/a$, a being the lattice spacing. $\mathbf{k}' = \mathbf{k} - \mathbf{K}$. A factor of 2 accounts for the contribution of the two equivalent Fermi points. For small $\mathbf{q}$ and $\mathbf{k}'$, the EPC matrix elements in the numerator in Eq. (5) are

$$|g^{LO/TO}_{(\mathbf{K}+\mathbf{k}'+\mathbf{q})\pi^*,(\mathbf{K}+\mathbf{k}')\pi}|^2 = \langle g^2_\Gamma\rangle_{\mathrm{F}}[1 \pm \cos(\theta+\theta')], \quad (6)$$

where θ is the angle between $\mathbf{k}'$ and $\mathbf{q}$, and θ' is the angle between $\mathbf{k}'+\mathbf{q}$ and $\mathbf{q}$ [22]. The + or the − sign refers to the LO and the TO modes, respectively. In graphene, the electronic bands near the Fermi level have a conic shape. Therefore, for small $\mathbf{q}$ and $\mathbf{k}'$,

$$\epsilon_{\mathbf{K}+\mathbf{k}',\pi} - \epsilon_{\mathbf{K}+\mathbf{k}'+\mathbf{q},\pi^*} = -\beta k' - \beta|\mathbf{k}'+\mathbf{q}|, \quad (7)$$

where $\beta = 14.1$ eV is the slope of the π bands within GGA. Replacing Eqs. (5)–(7), in Eq. (3), one obtains

$$\alpha^{LO/TO}_\Gamma = \frac{4\sqrt{3}\langle g^2_\Gamma\rangle_{\mathrm{F}}}{\beta} \times \lim_{\mathbf{q}\to 0}\frac{1}{q}\int_{k'<k_{\mathrm{m}}} \times d^2k' \left[\frac{1 \pm \cos 2\theta}{2k'} - \frac{1 \pm \cos(\theta+\theta')}{k' + |\mathbf{k}'+\mathbf{q}|}\right] = \frac{4\sqrt{3}\langle g^2_\Gamma\rangle_{\mathrm{F}}}{\beta} \int_0^\infty dy \int_0^{2\pi} \times d\theta \left[\frac{1}{2} - \frac{y \pm y\cos(\theta+\theta')}{y + \sqrt{1+y^2+2y\cos\theta}}\right],$$

where $y = k/q$, and $\theta' = \arctan[y\sin\theta/(1+y\cos\theta)]$. The integral is zero for the TO mode and $\pi^2/4$ for the LO mode. Thus, as expected, $\alpha^{\mathrm{TO}}_\Gamma = 0$ and

$$\alpha^{\mathrm{LO}}_\Gamma = \sqrt{3}\pi^2\langle g^2_\Gamma\rangle_{\mathrm{F}}/\beta = 397\mathrm{cm}^{-1}. \quad (8)$$

For the $\mathbf{K}$ point, we consider transitions from the neighborhood of $\mathbf{K}$ to the neighborhood of $2\mathbf{K}$. The EPC matrix elements are

$$|g_{(2\mathbf{K}+\mathbf{k}'+\mathbf{q}')\pi^*,(\mathbf{K}+\mathbf{k}')\pi}|^2 = \langle g^2_{\mathbf{K}}\rangle_{\mathrm{F}}(1+\cos\theta''), \quad (9)$$

with θ'' the angle between $\mathbf{k}'$ and $\mathbf{k}'+\mathbf{q}'$ [22]. Equation (4) becomes

$$\alpha_{\mathbf{K}} = \frac{2\sqrt{3}\langle g^2_{\mathbf{K}}\rangle_{\mathrm{F}}}{\beta} \lim_{\mathbf{q}'\to 0}\frac{1}{q'}\int_{k'<k_{\mathrm{m}}} d^2k' \left[\frac{1}{k'} - \frac{1+\cos\theta''}{k'+|\mathbf{k}'+\mathbf{q}'|}\right].$$

The limit of the integral is $\pi^2/2$, and therefore

$$\alpha_{\mathbf{K}} = \sqrt{3}\pi^2\langle g^2_{\mathbf{K}}\rangle_{\mathrm{F}}/\beta = 973\mathrm{cm}^{-1}. \quad (10)$$

The resulting linear dispersions are plotted in Figs. 1 and 2 . As expected, the phonon slopes near the discontinuities are very well reproduced. Finally, we note that, within a first-neighbors tight-binding (TB) approximation, the EPCs at Γ and $\mathbf{K}$ are not independent, since

$$(\langle g^2_{\mathbf{K}}\rangle_{\mathrm{F}}\omega_{\mathbf{K}})/(\langle g^2_\Gamma\rangle_{\mathrm{F}}\omega_\Gamma) = 2. \quad (11)$$

The validity of this relation is supported by our DFT result, for which $(\langle g^2_{\mathbf{K}}\rangle_{\mathrm{F}}\omega_{\mathbf{K}})/(\langle g^2_\Gamma\rangle_{\mathrm{F}}\omega_\Gamma) = 2.02$.

Equations (8) and (10) allow us to directly measure the EPCs at Γ and $\mathbf{K}$ from the experimental phonon slopes. The phonon branches around Γ have been measured by several groups with close data agreement [13]. The fit for $q \leq 0.15$ of the measurements in Fig. 1 [9], with $\hbar\omega_{\mathbf{q}} = \hbar\omega_\Gamma + \alpha^{\mathrm{LO}}_\Gamma q + \gamma q^2$, gives $\alpha^{\mathrm{LO}}_\Gamma = 340\ \mathrm{cm}^{-1}$, and $\langle g^2_\Gamma\rangle_{\mathrm{F}} = 0.035\ \mathrm{eV}^2$ [23]. The available data around $\mathbf{K}$ are much

more scattered. However, from Eq. (11) we get $\langle g^2_{\mathbf{K}}\rangle_{\mathrm{F}} = 0.086\ \mathrm{eV}^2$. These values are in excellent agreement with our calculations and validate our results.

The EPCs near **K** between π^* bands [24] allow the accurate determination of the intensity and shape of the Raman *D* peak. This will be the topic of future publications. Here, we remark that the A'_1 branch has the biggest $\langle g^2_{\mathbf{K}}\rangle_{\mathrm{F}}$ amongst **K** phonons. Thus, the *D* peak is due to the highest optical branch starting from the **K**-A'_1 mode [4,9–11], not to the branch starting from the **K**-E' mode, as in [5–8,12]. Also, the *D* peak shifts linearly with laser excitation energy ($\sim 50\ \mathrm{cm}^{-1}/\mathrm{eV}$ [12]). This is at odds with the flat slope of the **K**-A'_1 branch obtained by previous calculations [6–8,10,13,14]. But it is consistent with the **K**-A'_1 linear dispersion we get. The *D* peak dispersion reflects the slope of the Kohn anomaly at **K** and provides another independent measure of the EPCs. From Ref. [5], for $q' \to 0$, the *D* peak dispersion is $\sim \alpha_{\mathbf{K}}/\beta$. This gives $\langle g^2_{\mathbf{K}}\rangle_{\mathrm{F}} \sim 0.072\ \mathrm{eV}^2$ and, from Eq. (11), $\langle g^2_{\Gamma}\rangle_{\mathrm{F}} \sim 0.029\ \mathrm{eV}^2$. The EPCs derived in this way are a lower limit since the experimental *D* peak dispersion is measured with laser excitation energies ≥ 1 eV [12]. This corresponds to the phonon slope at $q' \geq 0.035$, which, from Fig. 2, underestimates by 30% the slope at $q' = 0$. Taking this into account, the EPCs independently inferred from the *D* peak dispersion are as well in excellent agreement with our calculations.

Because of the reduced dimensionality, we predict even stronger Kohn anomalies for metallic CNTs, and no anomaly for semiconducting CNTs. This is the key to differentiate the electrical nature of CNTs by Raman. A softening of CNT phonons corresponding to the graphene Γ-E_{2g} mode was recently reported [14]. We expect a stronger softening for the phonons corresponding to the graphene **K**-A'_1 mode, since $\langle g^2_{\mathbf{K}}\rangle_{\mathrm{F}} > \langle g^2_{\Gamma}\rangle_{\mathrm{F}}$.

In conclusion, we demonstrated two remarkable Kohn anomalies in the phonon dispersions of graphite, revealed by two kinks for the Γ-E_{2g} and **K**-A'_1 modes. Even if Kohn anomalies were observed in many materials [17], graphite is the first real material where a simple analytic description of the anomaly is possible. Indeed, we proved, by an exact analytic derivation, that the slope of the kinks is proportional to the ratio between the EPC matrix elements square and the π bands slope at the Fermi energy. As a consequence, we directly derived the EPCs at Γ and **K** from the experimental phonon dispersions. The values we obtain are in excellent agreement with calculations. Finally, our $\langle g^2_{\Gamma}\rangle_{\mathrm{F}}$ and $\langle g^2_{\mathbf{K}}\rangle_{\mathrm{F}}$ values, with Eqs. (6) and (9), and [24], can be used to determine the mean free path for electron scattering by optical phonons. This gives the limit of ballistic transport in CNTs and is of great scientific and technologic importance [2]. This calculation can be done, within the folding model, using the Fermi golden rule, and will be reported elsewhere.

We thank C. Brouder, M. Calandra, and S. Reich for useful discussions. Calculations were performed at HPCF (Cambridge) and IDRIS (Orsay) using PWSCF [25]. S. P. was supported by the EU project FAMOUS and the Marie Curie Fellowship IHP-HPMT-CT-2000-00209. A. C. F. acknowledges funding from the Royal Society.

[1] C. T. White, T. N. Todorov, Nature (London) **393**, 240 (1998).
[2] Z. Yao *et al.*, Phys. Rev. Lett. **84**, 2941 (2000); A. Javey *et al.* Phys. Rev. Lett. **92**, 106804 (2004).
[3] A. M. Rao *et al.* Science **275**, 187 (1997).
[4] A. C. Ferrari and J. Robertson Phys. Rev. B **61**, 14 095 (2000); **64**, 075414 (2001).
[5] C. Thomsen and S. Reich Phys. Rev. Lett. **85**, 5214 (2000).
[6] M. J. Matthews *et al.* Phys. Rev. B **59**, 6585 (1999).
[7] A. Grüneis *et al.*. Phys. Rev. B **65**, 155405 (2002).
[8] R. Saito *et al.* Phys. Rev. Lett. **88**, 027401 (2002).
[9] J. Maultzsch *et al.*. Phys. Rev. Lett. **92**, 075501 (2004).
[10] C. Mapelli *et al.*. Phys. Rev. B **60**, 12 710 (1999); C. Castiglioni *et al.*, Synth. Met. **139**, 885 (2003).
[11] F. Tuinstra and L. J. Koenig J. Chem. Phys. **53**, 1126 (1970).
[12] I. Pocsik *et al.* J. Non-Cryst. Solids **227-230**, 1083 (1998).
[13] G. Kresse *et al.* Europhys. Lett. **32**, 729 (1995); P. Pavone *et al.* Physica B (Amsterdam) **219-220**, 439 (1996); for a review see,L. Wirtz and A. Rubio, Solid State Commun. **131**, 141 (2004).
[14] O. Dubay and G. Kresse, Phys. Rev. B **67**, 035401 (2003).
[15] W. Kohn Phys. Rev. Lett. **2**, 393 (1959).
[16] J. P. Perdew *et al.*, Phys. Rev. Lett. **77**, 3865 (1996).
[17] S. Baroni *et al.* Rev. Mod. Phys. **73**, 515 (2001).
[18] N. Troullier and J. L. Martins Phys. Rev. B **43**, 1993 (1991).
[19] M. Methfessel and A. T. Paxton Phys. Rev. B **40**, 3616 (1989). We used a Hermite-Gauss smearing of an order of 1. For graphene we use a $32 \times 32 \times 1$ BZ grid for $\sigma \geq 0.02$ Ry, and a $64 \times 64 \times 1$ for $\sigma = 0.01$ Ry. For graphite we use $32 \times 32 \times 4$ with $\sigma = 0.02$ Ry. With these parameters, the frequencies converge to less than 1 cm^{-1}.
[20] A. Shukla *et al.*, Phys. Rev. Lett. **90**, 095506 (2003); at the *A* point $J_{\mathbf{q}} = 0.625(\mathrm{eV})^{-2}$.
[21] $\Delta n_{\mathbf{q}}$ is also nonanalytic in **q**. E.g., at Γ, at the lowest order, $\Delta n_{\mathbf{q}} - \Delta n_{\Gamma}$ is proportional to q. However, the nonanalyticity of $\Delta n_{\mathbf{q}}$ gives a contribution to $D_{\mathbf{q}} - D_{\Gamma}$ of order q^2, since Eq. (2) is stationary with respect to $\Delta n_{\mathbf{q}}$.
[22] This angular dependence was derived using a simple tight-binding model and reproduces very accurately the behavior of our fully *ab initio* calculations.
[23] In contrast, a much smaller $\langle g^2_{\Gamma}\rangle_{\mathrm{F}} \sim 0.003\ \mathrm{eV}^2$ was recently derived with a tight-binding model in J. Jiang *et al.*, Chem. Phys. Lett. **392**, 383 (2004).
[24] For the branch near A'_1 at **K**, $|g_{(2\mathbf{K}+\mathbf{k}'+\mathbf{q}')\pi^*,(\mathbf{K}+\mathbf{k}')\pi^*}|^2 = \langle g^2_{\mathbf{K}}\rangle_{\mathrm{F}}(1-\cos\theta'')$. For the branches near the E_{2g} at Γ $|g^{\mathrm{LO/TO}}_{(\mathbf{K}+\mathbf{k}'+\mathbf{q})\pi^*,(\mathbf{K}+\mathbf{k}')\pi^*}|^2 = \langle g^2_{\Gamma}\rangle_{\mathrm{F}}[1 \mp \cos(\theta+\theta')]$.
[25] S. Baroni *et al.* http://www.pwscf.org.